AIP | Applied Physics Letters

Spatially resolved photocurrents in graphene nanoribbon devices

Eberhard Ulrich Stützel, Thomas Dufaux, Adarsh Sagar, Stephan Rauschenbach, Kannan Balasubramanian et al.

Citation: Appl. Phys. Lett. **102**, 043106 (2013); doi: 10.1063/1.4789850
View online: http://dx.doi.org/10.1063/1.4789850
View Table of Contents: http://apl.aip.org/resource/1/APPLAB/v102/i4
Published by the American Institute of Physics.

Spatially resolved photocurrents in graphene nanoribbon devices

Eberhard Ulrich Stützel,[1,a)] Thomas Dufaux,[1] Adarsh Sagar,[1] Stephan Rauschenbach,[1] Kannan Balasubramanian,[1] Marko Burghard,[1,a)] and Klaus Kern[1,2]
[1]*Max Planck Institute for Solid State Research, Heisenbergstrasse 1, D-70569 Stuttgart, Germany*
[2]*Institut de Physique de la Matière Condensée, Ecole Polytechnique Fédérale de Lausanne, 1015 Lausanne, Switzerland*

(Received 14 November 2012; accepted 11 January 2013; published online 29 January 2013)

We present here a scanning photocurrent microscopy study of individual graphene nanoribbons, revealing pronounced photocurrent responses close to the nanoribbon/metal contacts. The magnitude of the corresponding photocurrent signal was found to be directly proportional to the conductance of the devices, suggesting that a local voltage source is generated at the nanoribbon/metal interface by the photo-thermoelectric Seebeck effect. The dominance of this mechanism is attributed to the reduced thermal conduction capability of the nanoribbons in comparison to extended graphene sheets. © *2013 American Institute of Physics*. [http://dx.doi.org/10.1063/1.4789850]

Graphene exhibits excellent charge transport properties which emerge from its unique two-dimensional energy dispersion of massless Dirac fermions. This feature has triggered numerous studies directed toward its rich fundamental physics and manifold potential applications.[1] Of particular interest for device applications is graphene's high carrier mobility and ballistic transport.[2–5] However, due to the absence of a band gap in graphene and the formation of electron-hole puddles, graphene-based field effect transistors (FETs) cannot be turned off.[6] One strategy to increase the on/off ratio relies on patterning graphene in narrow stripes, thereby introducing a band gap into the resulting graphene nanoribbons (GNRs).[7,8] The synthesis of GNRs has been achieved through various methods, including chemical vapor deposition, gas-phase chemical/plasma etching, or unzipping of carbon nanotubes (CNTs).[9–11] The electrical performance of devices fabricated from such GNRs turned out to vary greatly depending on the experimental conditions, in particular the chemical environment during the fabrication process. For instance, the conductance of GNRs obtained via oxygen plasma etching of graphene using a silicon nanowire mask has been reported to be 10^{-5} S.[12] By comparison, at least one order of magnitude lower values have been found for GNRs produced by unzipping CNTs using a solution-based chemical oxidative process.[13,14] The lower conductance in the latter case has been attributed to the presence of functional groups (e.g., carboxylic or hydroxyl groups) at the edges of the GNRs. Thus, it is highly desirable to study GNRs which owing to their high structural quality display reproducible electrical properties.

More recently, also the optoelectronic properties of pristine or patterned graphene have received strong attention.[15] For example, graphene has been experimentally studied as a component of mode-locked lasers or ultrafast photodetectors.[16–18] On the more fundamental side, the photocurrent generation at the graphene/metal or graphene monolayer/bilayer interface has been explored.[19–24] Furthermore, the photoresponse of graphene p-n junctions, created by chemical or electrostatic doping,[25,26] as well as the speed limit of graphene-based photodetectors have been investigated.[27,28] With regard to GNRs, although their dark electrical properties have been experimentally investigated to some extent,[7,8,10,29,30] their optoelectronic behavior has thus far been addressed only by theory.[31] Here, we use scanning photocurrent microscopy (SPCM) to study the spatially resolved photocurrent response of individual GNRs. In contrast to extended graphene sheets, in our experiments the entire width of the conducting channel (GNR width ~10 to 20 nm) is illuminated by the laser spot (~500 nm diameter) such that potential complications due to inhomogeneous temperature and/or electric field gradients over the channel width are effectively avoided.

The GNRs were fabricated using CdSe nanowires (NWs) as etching masks (see Figures 1(a)–1(c)). Graphene was mechanically exfoliated from highly oriented pyrolytic graphite onto highly doped Si substrates coated with a 300 nm thick thermally grown SiO_2 layer by the scotch tape method.[1] Several μm long and 10–35 nm wide CdSe NWs were grown by the solution-liquid-solid method.[32] A dispersion of CdSe NWs in chloroform was prepared by removing excess trioctylphosphine oxide (TOPO) via centrifugation (Eppendorf 5417C) for 10 min at 10 000 rpm and subsequent re-dispersion in the pure solvent, which was repeated two times. The resulting CdSe NW dispersion was drop-casted onto the graphene-coated Si/SiO_2 substrates placed on a hotplate at 50 °C (Figure 1(a)). Afterwards, the substrates were rinsed with chloroform for 15 s in order to remove excess CdSe NWs and TOPO. Subsequently, they were heated under argon atmosphere to 120 °C for 10 min, with the aim of improving the adhesion between the CdSe NWs and graphene. The location of single CdSe NWs and their corresponding height was determined by tapping mode atomic force microscopy (AFM). The presence of monolayers was confirmed by confocal Raman microscopy using $\lambda = 488$ nm and a power of 0.7 mW (see Figure S5 in supplementary material).[33,34] Subsequently, reactive ion etching (RIE) (Leybold LE 301) was performed to etch away only a few layers of graphene around individual NWs (Figure 1(b)) (5 s, 100 sccm Ar, 11 sccm O_2, 0.05 mbar, 48 W). The CdSe NWs

a)Authors to whom correspondence should be addressed. Electronic addresses: E.Stuetzel@fkf.mpg.de and M.Burghard@fkf.mpg.de.

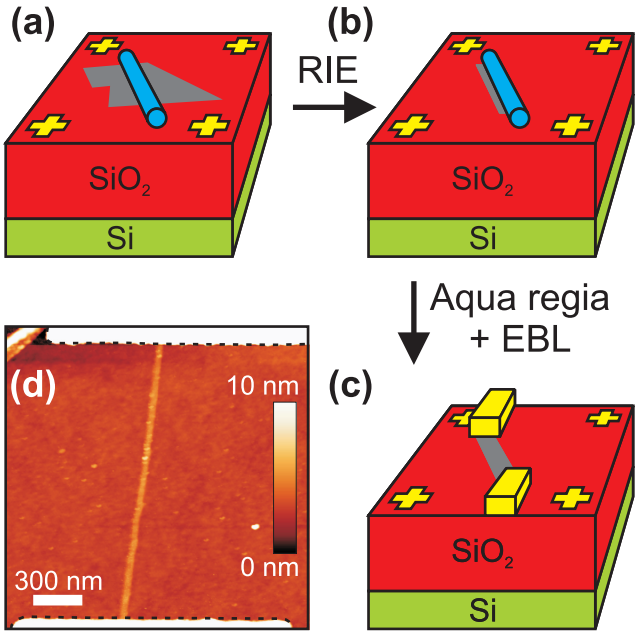

FIG. 1. Flowchart of the graphene nanoribbon device fabrication. (a) Mechanical exfoliation of graphene onto a Si/SiO_2 substrate with markers, followed by deposition of CdSe nanowires. (b) The wires serve as etching mask during subsequent reactive ion etching. (c) After wet etching of the wires, the ribbons are provided with metal contacts. (d) AFM image of a 22 nm wide GNR device. The distance in between the contacts is 1.5 μm.

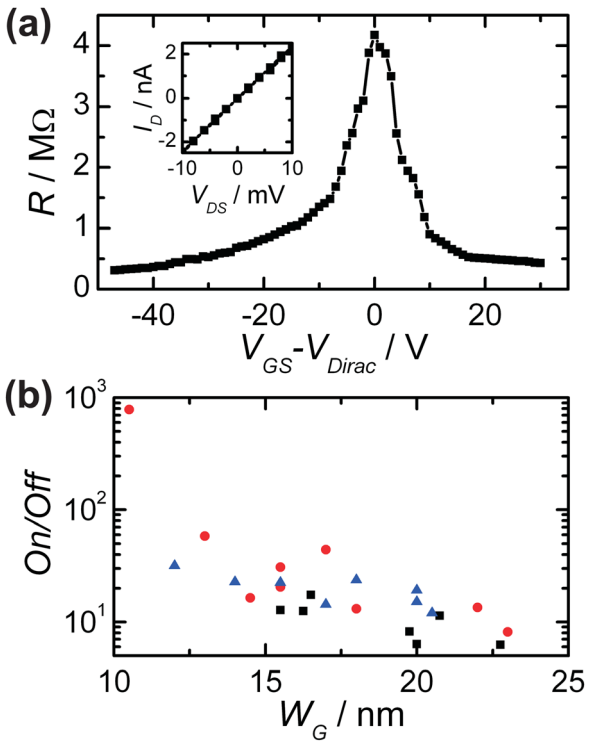

FIG. 2. Electrical characterization of GNR devices under ambient conditions. (a) Electrical resistance as a function of V_{GS} for the device shown in Fig. 1(d) ($V_{Dirac} = +10$ V in this case). Inset: I_D vs. V_{DS} curve at the Dirac point. (b) On/off ratio plotted against ribbon width. The on conductance is measured in the p-type regime at V_{GS}-$V_{Dirac} = -30$ V. In total 24 GNR devices on three different chips (assigned by black squares, red circles, and blue triangles, respectively) were evaluated.

were completely dissolved by dipping the substrates into a mixture of 20 ml of 30% HCl + 1 ml of 69% HNO_3 for 3 s at room temperature, followed by rinsing with deionized (DI) water, dipping into an aqueous solution of sodium sulfide (1.2 g Na_2S + 2.5 ml H_2O) for 30 s at room temperature, and finally rinsing with DI-water.[35] This procedure was repeated two more times, followed by rinsing with isopropanol and blowing dry under a stream of argon. Metal contacts were then defined by e-beam lithography and thermal evaporation of either 20 nm Ti + 20 nm Au or 2 nm Cr + 40 nm Pd (Figure 1(c)). As shown in Figure S1 of supplementary material[34] the width of the GNRs agrees well with the diameter of the corresponding NWs. The exemplary AFM image in Figure 1(d) testifies a regular structure and clean surface of the resulting GNRs.

Electrical transport and photocurrent measurements were performed under ambient conditions. In all photocurrent measurements, no drain-source voltage was applied (except the control measurements shown in Figure S4 of supplementary material[34]). A confocal microscope (Leica TCS SP2, 50× objective with NA 0.8) was utilized in the SPCM experiments, wherein the samples were raster-scanned through the approximately 500 nm wide laser spot (linearly polarized light with $\lambda = 633$ nm and a power of 240 μW was used to ensure a good signal-to-noise ratio). The photocurrent and AFM images were evaluated and processed using WSXM.[36]

The devices were electrically characterized under ambient conditions in conventional FET configuration using the doped silicon substrate as a back gate. In general, the I_D vs. V_{DS} curves showed a linear dependence, as exemplified by the inset in Figure 2(a) for the GNR in Figure 1(d). From the transfer curves revealing ambipolar behavior, an on/off ratio can be determined by dividing the resistance at the Dirac point by the resistance determined well within the p-type regime (at V_{GS}-$V_{Dirac} = -30$ V).[37] For the present device with $V_{Dirac} = +10$ V, an on/off ratio of 14 is obtained. Figure 2(b) shows the dependence of the on/off ratio on the ribbon width, W_G, for, in total, 24 different GNR devices. With decreasing width, the on/off ratio increases, reaching almost 3 orders of magnitude for a ~10 nm wide GNR. This trend is consistent with the opening of a transport energy gap E_{gap}, which is inversely proportional to W_G, $E_{gap} \sim W_G^{-1}$ ($G_{on}/G_{off} \sim \exp^{E_{gap}/kT}$).[7,8,29,38] The obtained on-resistance values and on/off ratios agree well with previous reports on GNRs with comparable widths.[29,37,39] It is hence concluded that the removal of the CdSe NWs does not deteriorate the electrical transport properties of the GNRs, which is further corroborated by the fact that the charge neutrality point remains close to zero gate voltage (see Figure S2 of supplementary material[34]). This behavior is distinguished from other cases like exposure to the e-beam resist HSQ, whereby additional scattering or doping is introduced.[40]

Spatially resolved photoresponse of the GNRs was measured by SPCM, wherein an unbiased device is raster-scanned (lateral step size of ~60 nm) through a confocal laser spot ($\lambda = 633$ nm), while recording the electrical current for each position. The employed set-up is schematically depicted in Figure S3 of supplementary material.[34] An optical reflection image of the device in Figure 1(d) is displayed in Figure 3(a), where due to the low reflection intensity of the GNR only the electrodes can be discerned. As illustrated

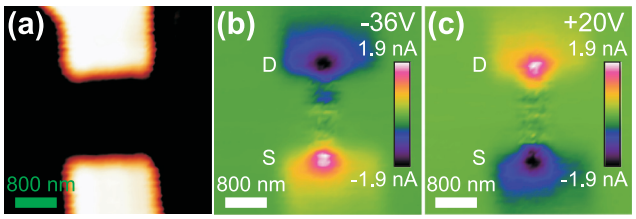

FIG. 3. SPCM measurements of the device in Fig. 1(d) (step size ~62 nm). (a) Optical reflection image recorded during the photocurrent measurement, revealing the two metal contacts. (b) SPCM image in the p-type regime of the device (V_{GS}-$V_{Dirac} = -36$ V, $V_{DS} = 0$ V). The two photocurrent peaks are, respectively, denoted as S and D, according to their nearby electrodes. (c) SPCM image recorded in the n-type regime at V_{GS}-$V_{Dirac} = +20$ V.

by Figure 3(b), in the p-type regime (gate-source voltage V_{GS}-$V_{Dirac} = -36$ V, $V_{DS} = 0$ V) a positive photocurrent of ~2 nA is observed at the source contact, while a negative current of similar magnitude occurs at the drain contact. Upon transition from the p-type to the n-type regime (i.e., by applying a positive gate-source voltage), the photocurrent at the source contact changes sign from positive to negative, while a positive current emerges at the drain contact, as illustrated in Figure 3(c). Such sign reversal of the photocurrent signals is well-documented for graphene.[19–22] It is noteworthy that in all GNR devices no difference could be observed between parallel and perpendicular polarization direction of the incident laser light with respect to the long axis of the GNR. This finding is in contrast to the report of Shi *et al.*[41] Most likely due to the fact that in the latter work nanogap electrodes were used as plasmonic antenna.

Photocurrent generation in extended graphene has been attributed to the presence of a local built-in electric field which separates photoexcited electron-hole pairs.[19–22,24] Such fields are typically present at the electrical contacts, and their magnitude depends on the difference in the work functions of the contact metal and the graphene. To evaluate whether this mechanism can explain the photocurrent generation at the GNR/metal junction, we compare the corresponding local photocurrent signals detected from GNRs with different dimensions. In order to exclude the influence of different charge carrier concentrations in the devices, the comparison is made at high carrier densities in the p- or n-type regime. The photocurrent caused by the built-in field is given by $I_{Photo} = W_G \times e \times n^* \times \xi$, where e is the elementary charge, n^* the photoinduced carrier density, and ξ the built-in field.[42,43] It is noteworthy that the light power per area should be constant over the GNR width W_G, as the latter is much smaller compared to the approximately 500 nm wide laser spot. For both gating regimes, the plots of the measured photocurrent as a function of W_G (see Figure 4(a)) display a pronounced scatter rather than a linear dependence. This observation is incompatible with the built-in field mechanism, although it may be argued that work function differences between the GNR devices could have a profound influence. However, this scenario is unlikely considering the fact that even GNRs with the same width and on/off ratio exhibit notably different photocurrents, as apparent from Table SI. This conclusion remains valid also when partial recombination of the excited carriers is taken into account (see supplementary material[34]).[43]

In contrast to the plot of I_{Photo} vs. W_G, a linear dependency can be observed between I_{Photo} and the inverse resistance of the GNRs (see Figure 4(b)). The photocurrent rises linearly with the inverse resistance, with an overall increase by a factor of approximately 10 in both cases. It turns out that very similar photovoltage values are obtained by multiplying the (dark) electrical resistance at a fixed gate-source voltage $R(V_{GS})$ with the photocurrent peak magnitude $I_{Photo}(V_{GS})$ under the same condition, as shown by the corresponding plots in Figure 4(b). Here, $R(V_{GS})$ is assumed to be independent of laser illumination, which is justified by experiment (see Figure S4 of supplementary material[34]). The observation of an almost constant photovoltage close to the contacts (see equivalent circuit in Figure 4(c)) points toward the photo-thermoelectric Seebeck effect as the dominant mechanism responsible for the

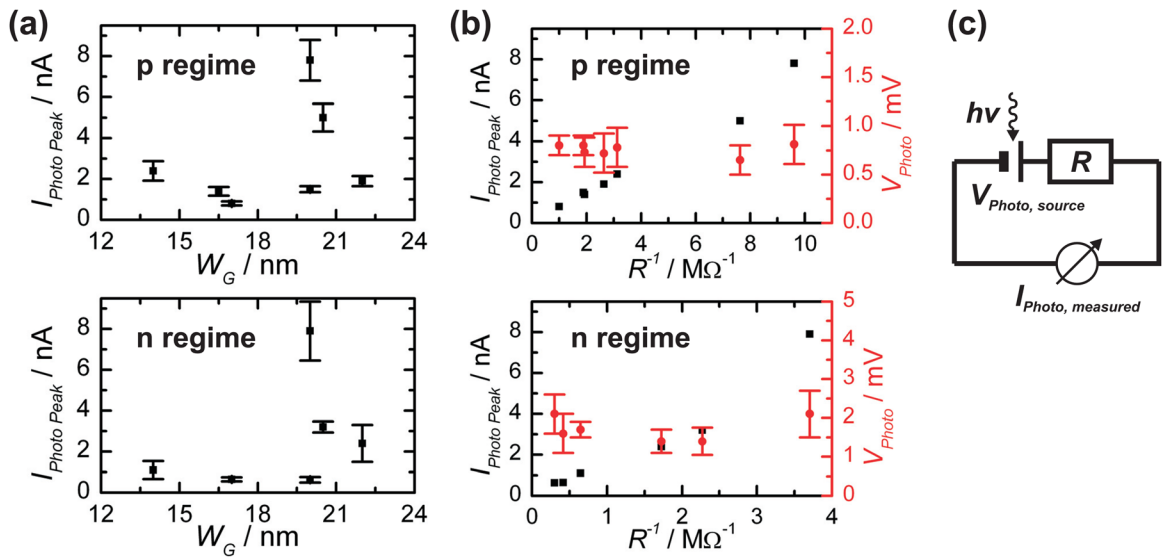

FIG. 4. (a) Photocurrent detected close to the metal contact in dependence of the GNR width. The gate voltage was adjusted to $V_{GS} \sim -30$ V for the p-type regime, and $V_{GS} \sim +30$ V in the case of n-type regime. Error bars correspond to the standard deviation by averaging over several measurements. (b) Photocurrent (black squares) and calculated photovoltage values (red circles) in dependence of the inverse of the measured ohmic resistance of several GNR devices. (c) Equivalent circuit model to account for the results in panel (b).

photocurrent generation. This mechanism has been invoked as an alternative to the built-in electric field to explain the photocurrent generation at the graphene/metal or graphene monolayer/bilayer interface, or graphene p-n junctions.[21,23,24,26] It relies upon the existence of a temperature difference ΔT between the two graphene/metal interfaces, one of which is locally heated by the laser spot. This produces a thermoelectric voltage $V = (S_G - S_{Metal}) \times \Delta T$, where S_G and S_{Metal} is the Seebeck coefficient of the GNR and contact metal, respectively. As a consequence, a thermoelectrically induced photocurrent is generated whose magnitude scales inversely with the GNR device resistance $I_{Photo} = V_{Photo}/R$.

The Seebeck coefficient S_G can be estimated from the Mott relation: $S_G = -\pi^2 k_B{}^2 T/3\, e \times 1/\sigma \times d\sigma/dV_{GS} \times \mathrm{d}V_{GS}/dE$.[44,45] As the two-probe resistance R and dR/dV_{GS} both depend on the contact resistance of the devices, we derive the magnitude of the latter by fitting $R(V_{GS})$ for holes and electrons separately[46] and subtract it from R. In this manner, one obtains respective values of $S \approx +30\,\mu$V/K and $S \approx -40\,\mu$V/K for the p- and n-type regime of the device in Figure 1(d). The finding of a larger Seebeck coefficient in the n- vs. p-type regime is in accord with previous reports and is explainable by the electron-hole asymmetry introduced by contact doping.[44,47] The present S values are slightly smaller than the $\sim 50\,\mu$V/K reported for graphene, which could be explained by the better gate coupling in the GNR devices.[44] The measured photovoltages of 0.76 mV in the p-type and 1.7 mV in the n-type regime yield a respective temperature difference ΔT of $\sim$30 K and $\sim$40 K between the illuminated region at the GNR/metal interface and the surrounding. The notable difference between the two gating regimes is at least partly due to neglecting S_{Metal}. Interestingly, the above ΔT range significantly exceeds that of $\Delta T \approx 0.1$-1 K obtained for graphene using comparable laser wavelengths and a power of 40 μW.[23,26] This difference cannot be fully accounted for by the higher laser power of 240 μW used in the present experiments, which suggests a reduced heat transport capability of the GNRs in comparison to graphene.[48] Heat dissipation is dominated by the SiO_2 substrate and/or the metal contacts rather than the GNR itself.[48] This hypothesis is supported by a comparison with Raman spectroscopy studies on GNRs. Prolonged irradiation ($\lambda = 633$ nm, 300 kW/cm^2 intensity) causes photoinduced changes, similar to the effect of thermal heating to 100 °C in air.[49] Hence, a few tens of Kelvin seem to be reasonable for our setup (120 kW/cm^2). However, it should be emphasized that even if photocurrent generation in GNRs is predominantly via the photo-thermoelectric mechanism, the situation may be different for extended sheets of graphene, in which heat dissipation is more effective.

In conclusion, narrow GNRs of high structural quality have been obtained using CdSe NWs as an etching mask. The photocurrent measured in proximity of the metal contacts to the GNRs was found to rise linearly with increasing electrical conductance of the nanoribbons. This behavior can be well explained by a local voltage source induced by the photo-thermoelectric Seebeck effect. The photovoltage generation is intimately connected to the pronounced local heating of the GNRs by the laser spot, as distinguished from the case of more efficient heat transport in extended graphene sheets. This finding needs to be considered in the development of graphene-based optoelectronic devices wherein the geometrical design plays an important role.

This work was supported by the Deutsche Forschungsgemeinschaft (DFG) in the framework of the SPP 1459—Graphene (BU 1125/8). The authors thank E. Peters, Dr. T. Lutz, G. Rinke, and M. Esslinger for valuable discussions. A. Mews and Z. Wang are acknowledged for providing CdSe nanowires. We are grateful to B. Krauss for support with the Raman setup, M. Hagel and T. Reindl with the etching experiments, as well as P. Gehring for scanning electron microscopy measurements.

[1]K. S. Novoselov, A. K. Geim, S. V. Morozov, D. Jiang, Y. Zhang, S. V. Dubonos, I. V. Grigorieva, and A. A. Firsov, Science **306**, 666 (2004).
[2]K. I. Bolotin, K. J. Sikes, Z. Jiang, M. Klima, G. Fudenberg, J. Hone, P. Kim, and H. L. Stormer, Solid State Commun. **146**, 351 (2008).
[3]X. Du, I. Skachko, A. Barker, and E. Y. Andrei, Nat. Nanotechnol. **3**, 491 (2008).
[4]X. Hong, A. Posadas, K. Zou, C. H. Ahn, and J. Zhu, Phys. Rev. Lett. **102**, 136808 (2009).
[5]C. R. Dean, A. F. Young, I. Meric, C. Lee, L. Wang, S. Sorgenfrei, K. Watanabe, T. Taniguchi, P. Kim, K. L. Shepard, and J. Hone, Nat. Nanotechnol. **5**, 722 (2010).
[6]J. Martin, N. Akerman, G. Ulbricht, T. Lohmann, J. H. Smet, K. von Kltizing, and A. Yacoby, Nat. Phys. **4**, 144 (2008).
[7]M. Y. Han, B. Özyilmaz, Y. Zhang, and P. Kim, Phys. Rev. Lett. **98**, 206805 (2007).
[8]Z. Chen, Y. M. Lin, M. J. Rooks, and P. Avouris, Physica E **40**, 228 (2007).
[9]T. Kato and R. Hatakeyama, Nat. Nanotechnol. **7**, 651 (2012).
[10]L. Jiao, L. Zhang, X. Wang, G. Diankov, and H. Dai, Nature (London) **458**, 877 (2009).
[11]L. Jiao, X. Wang, G. Diankov, H. Wang, and H. Dai, Nat. Nanotechnol. **5**, 321 (2010).
[12]J. Bai, R. Cheng, F. Xiu, L. Liao, M. Wang, A. Shailos, K. L. Wang, Y. Huang, and X. Duan, Nat. Nanotechnol. **5**, 655 (2010).
[13]D. V. Kosynkin, A. L. Higginbotham, A. Sinitskii, J. R. Lomeda, A. Dimiev, B. K. Price, and J. M. Tour, Nature (London) **458**, 872 (2009).
[14]T. Shimizu, J. Haruyama, D. C. Marcano, D. V. Kosinkin, J. M. Tour, K. Hirose, and K. Suenaga, Nat. Nanotechnol. **6**, 45 (2011).
[15]F. Bonaccorso, Z. Sun, T. Hasan, and A. C. Ferrari, Nat. Photonics **4**, 611 (2010).
[16]H. Zhang, Q. Bao, D. Tang, L. Zhao, and K. Loh, Appl. Phys. Lett. **95**, 141103 (2009).
[17]F. Xia, T. Mueller, Y. M. Lin, A. Valdes-Garcia, and P. Avouris, Nat. Nanotechnol. **4**, 839 (2009).
[18]T. Mueller, F. Xia, and P. Avouris, Nat. Photonics **4**, 297 (2010).
[19]E. J. H. Lee, K. Balasubramanian, R. T. Weitz, M. Burghard, and K. Kern, Nat. Nanotechnol. **3**, 486 (2008).
[20]F. Xia, T. Mueller, R. Golizadeh-Mojarad, M. Freitag, Y. M. Lin, J. Tsang, V. Perebeinos, and P. Avouris, Nano Lett. **9**, 1039 (2009).
[21]J. Park, Y. H. Ahn, and C. Ruiz-Vargas, Nano Lett. **9**, 1742 (2009).
[22]T. Mueller, F. Xia, M. Freitag, J. Tsang, and P. Avouris, Phys. Rev. B **79**, 245430 (2009).
[23]X. Xu, N. M. Gabor, J. S. Alden, A. M. van der Zande, and P. L. McEuen, Nano Lett. **10**, 562 (2010).
[24]L. Prechtel, L. Song, D. Schuh, P. Ajayan, W. Wegscheider, and A. W. Holleitner, Nat. Commun. **3**, 1 (2012).
[25]E. C. Peters, E. J. H. Lee, M. Burghard, and K. Kern, Appl. Phys. Lett. **97**, 193102 (2010).
[26]M. C. Lemme, F. H. L. Koppens, A. L. Falk, M. S. Rudner, H. Park, L. S. Levitov, and C. M. Marcus, Nano Lett. **11**, 4134 (2011).
[27]A. Urich, K. Unterrainer, and T. Mueller, Nano Lett. **11**, 2804 (2011).
[28]D. Sun, G. Aivazian, A. M. Jones, W. Yao, D. Cobden, and X. Xu, Nat. Nanotechnol. **7**, 114 (2012).
[29]J. Bai, X. Duan, and Y. Huang, Nano Lett. **9**, 2083 (2009).
[30]X. Li, X. Wang, L. Zhang, S. Lee, and H. Dai, Science **319**, 1229 (2008).

[31]V. Ryzhii, V. Mitin, M. Ryzhii, N. Ryabova, and T. Otsuji, Appl. Phys. Express **1**, 063002 (2008).
[32]Z. Li, A. Kornowski, A. Myalitsin, and A. Mews, Small **4**, 1698 (2008).
[33]A. C. Ferrari, J. C. Meyer, V. Scardaci, C. Casiraghi, M. Lazzeri, F. Mauri, S. Piscanec, D. Jiang, K. S. Novoselov, S. Roth, and A. K. Geim, Phys. Rev. Lett. **97**, 187401 (2006).
[34]See supplementary material at http://dx.doi.org/10.1063/1.4789850 for scanning electron microscopy images of GNR devices, transport measurement data with CdSe NW left on top, a scheme of the photocurrent setup, GNR photocurrent measurement data, transport measurement data for illumination, and Raman data.
[35]G. Hodes, Nature (London) **285**, 29 (1980).
[36]I. Horcas, R. Fernández, J. M. Gómez-Rodríguez, J. Colchero, J. Gómez-Herrero, and A. M. Baro, Rev. Sci. Instrum. **78**, 013705 (2007).
[37]G. Xu, C. M. Torres, Jr., J. Tang, J. Bai, E. B. Song, Y. Huang, X. Duan, Y. Zhang, and K. L. Wang, Nano Lett. **11**, 1082 (2011).
[38]Y. W. Son, M. L. Cohen, and S. G. Louie, Phys. Rev. Lett. **97**, 216803 (2006).
[39]Y. Lu, B. Goldsmith, D. R. Strachan, J. H. Lim, Z. Luo, and A. T. C. Johnson, Small **6**, 2748 (2010).
[40]Y. M. Lin, V. Perebeinos, Z. Chen, and P. Avouris, Phys. Rev. B **78**, 161409 (2008).
[41]S. F. Shi, X. Xu, D. C. Ralph, and P. L. McEuen, Nano Lett. **11**, 1814 (2011).
[42]S. M. Sze, *Physics of Semiconductor Devices* (Wiley-Interscience, New York, 1981), pp. 790–838.
[43]M. Freitag, T. Low, F. Xia, and P. Avouris, Nat. Photonics **7**, 53 (2013).
[44]Y. M. Zuev, W. Chang, and P. Kim, Phys. Rev. Lett. **102**, 096807 (2009).
[45]P. Wei, W. Bao, Y. Pu, C. N. Lau, and J. Shi, Phys. Rev. Lett. **102**, 166808 (2009).
[46]S. Kim, J. Nah, I. Jo, D. Shahrjerdi, L. Colombo, Z. Yao, E. Tutuc, and S. K. Banerjee, Appl. Phys. Lett. **94**, 062107 (2009).
[47]B. Huard, N. Stander, J. A. Sulpizio, and D. Goldhaber-Gordon, Phys. Rev. B **78**, 121402 (2008).
[48]A. D. Liao, J. Z. Wu, X. Wang, K. Tahy, D. Jena, H. Dai, and E. Pop, Phys. Rev. Lett. **106**, 256801 (2011).
[49]S. Ryu, J. Maultzsch, Y. M. Han, P. Kim, and L. E. Brus, ACS Nano **5**, 4123 (2011).